A&A 470, 1117–1122 (2007)
DOI: 10.1051/0004-6361:20066978

Astronomy & Astrophysics

Emission of electromagnetic waves by proton beams propagating in nonuniform solar plasmas

J. I. Sakai and Y. Nagasugi

Laboratory for Plasma Astrophysics, Faculty of Engineering, University of Toyama, 3190 Gofuku, Toyama 930-8555, Japan
e-mail: sakaijun@eng.u-toyama.ac.jp

Received 20 December 2006 / Accepted 24 April 2007

ABSTRACT

Aims. We investigate the dynamics of proton beams propagating along a uniform magnetic field, as well as across the magnetic field in nonuniform solar plasmas, paying attention to the emission process of electromagnetic waves. The aim is to understand a new solar-burst component emitting only in the terahertz range during the solar flare observed by Kaufmann et al. (2004, ApJ, 603, L121).
Methods. We used a 2D3V, fully relativistic, electromagnetic particle-in-cell (PIC) simulation.
Results. From the simulation where the proton beams propagate along a uniform magnetic field into the high-density region, we found that strong electromagnetic waves are generated behind the proton beams. When the proton beams propagate perpendicular to the magnetic field, we found that the extra-ordinary mode can be excited from two electron Bernstein waves through three-wave interactions. These simulation results could be applied to the electromagnetic wave emission from the solar photosphere during the solar flares.

Key words. plasmas – shock waves – Sun: flares – Sun: radio radiation– acceleration of particles

1. Introduction

Recently Kaufmann et al. (2004) reported the discovery of a new intense solar-flare spectral radiation component, peaking somewhere in the shorter submillimeter to far-infrared range, identified during the large 2003 November 4 flare. The new solar submillimeter telescope (SST; Kaufmann et al. 2001),designed to extend the frequency range of solar flare observations to above 100 GHz, was used to detect this new component with increasing flux between 212 and 405 GHz, appearing along with, but separated from, the well-known microwave emission component. The novel emission component had three major peaks with time, originating in a compact source whose position remained within 15″. Although the origin of the terahertz emission component during the flare is not known, it might be representative of emission due to electrons with energies that are considerably higher than those assumed to explain solar microwave emissions producing incoherent synchrotron radiation (ISR) with maximum spectral emission somewhere in the THz range.

Kaufmann & Raulin (2005) propose a new interpretation for the intense microwaves observed at the same time, assuming that the accelerated, ultrarelativistic electron beams undergo microbunching instabilities by producing broadband coherent synchrotron radiation (CSR) at microwaves, similar to what is observed in laboratory accelerators.

Recently Sakai et al. (2006b) investigated the new terahertz emission in terms of plasma emission mechanism. They assumed that relativistic electron beams (REBs) are generated during strong solar flares, although the origin of the REBs is not known. In contrast to mildly relativistic electrons for the solar type III bursts, they investigated the dynamics of relativistic electron beams propagating along a uniform magnetic field and the emission process of electromagnetic waves associated with the REBs. By using a 2D3V, fully relativistic, electromagnetic particle-in-cell (PIC) simulation, where the REBs propagate into the high-density region corresponding to the solar photosphere, they found that strong electromagnetic waves are generated behind the REBs. These simulation results could be applied to the electromagnetic wave emission with a terahertz frequency range from the solar photosphere during the solar flares.

On the other hand, it is well known that during strong solar flares, high-energy protons can be generated and that they are observed by gamma-ray emissions during the impulsive phase of solar flares. In most strong flare events, the time profile of the prompt gamma-ray line emission caused by energetic protons is observed to be very similar to that of the bremsstrahlung hard X-rays emitted by energetic electrons (Aschwanden 2002). This suggests that the acceleration and propagation of the flare-accelerated protons and electrons are closely related. The most typical event among them is the 1980 June 7 flare observed by the SMM (Forrest & Chupp 1983), that was explained by the current loop coalescence model (Tajima et al. 1982; Sakai & Ohsawa 1987; Sakai & De Jager 1996). Brown et al. (2000) suggest that hard X-rays in the flare impulsive phase are emitted by a neutralized proton beam due to the heating of the electrostatically dragged electrons.

Saito & Sakai (2004a,b) investigated the coalescence process of two parallel current loops with co-helicity by using a two-dimensional, electromagnetic, relativistic PIC code. They found that in a later stage of the two current loops coalescence, fast magnetosonic waves are generated as a result of rebound of the coalescence and they develop to shock waves. They also found that, near the fast magnetosonic shock front, the protons can be promptly accelerated by the shock surfing acceleration mechanism (Sagdeev & Shapiro 1973; Katsouleas & Dawson 1983). Recently Saito & Sakai (2006) found that during the formation of the current sheet, protons can be accelerated through the shock surfing mechanism by the fast magnetosonic shock

waves. It is also pointed out (Sakai et al. 2005, 2006a) that, during the type II radio bursts that can be produced from the fast magnetosonic shock waves, protons are also accelerated by the shock surfing mechanism.

Recently, Sakai et al. (2007) investigated the electromagnetic wave emission process from the proton beams produced by the fast magnetosonic shock waves. The proton velocity accelerated by the shock surfing mechanism reaches about $(m_p/m_e)^{1/2}(M_A-1)^{3/2}V_A$ (M_A is Alfvén Mach number), which becomes comparable to $c/3$. They found that the proton beams propagating to a low-density region from a high-density region are forced to move together with the electrons to keep charge neutrality, resulting in the excitation of electrostatic proton beam modes, as well as Langmuir waves. In the early stage of the excitation of the beam modes, both R and L modes near the fundamental plasma frequency can be emitted along a uniform magnetic field. They also found that the second harmonics of the electromagnetic waves can be excited in the late stage through the three-wave interactions. During these emission processes, proton beams can move along the magnetic field almost without losing their kinetic energy.

In the present paper we investigate the new terahertz emission in terms of a plasma emission mechanism, assuming that proton beams are generated during strong solar flares and propagate to the high-density region along the uniform magnetic field, as well as across the magnetic field. We find that strong electromagnetic waves are generated behind the proton beams. We find that the electromagnetic high-frequency emission in our simulation, which we consider to be the equivalent of the observed 405 GHz solar emission, has an intensity that is comparable to that of the low-frequency electromagnetic emission in our simulation. The latter would be the equivalent of the 212 GHz solar emission.

The shock surfing acceleration accelerates protons by the $v \times B$ force, and the protons gain energy perpendicular to the magnetic field. These beams will drive Buneman waves and lose their energy through electron surfing acceleration (Dieckmann & Shukla 2006). An oblique magnetic field can result in shock surfing acceleration, and here the protons can also gain a field-aligned velocity (Ucer & Shapiro 2005). Therefore we investigate how the emission process of the electromagnetic waves depends on the angle between the magnetic field and proton beams. We find that the electromagnetic waves can mostly be emitted independent of the angle between the magnetic field and proton beams, although the emission mechanism of the electromagnetic waves is different. These simulation results could be applied to the electromagnetic wave emission from the solar photosphere during the solar flares.

This paper is organized as follows. In Sect. 2 we show the simulation model and in Sect. 3 investigate the dynamics of the ion beams in non-uniform plasmas and present simulation results. In Sect. 4 we summarize our results.

2. Simulation model

We assume that proton beams are generated in the solar flare region by the surfatron acceleration process near the fast magnetosonic shock front. We investigate the emission process of electromagnetic waves when the proton beams propagate along a uniform magnetic field (y direction) from the flare region (low density) to the high-density region of the photosphere. We use a 2D3V, fully relativistic electromagnetic particle-in-cell (PIC) code, modified from a 3D3V, TRISTAN code (Buneman 1993). The system size is $L_x = 10\Delta$, $L_y = 6000\Delta$, where $\Delta(=1)$ is the grid size. The free boundary condition for y direction is imposed on particles and fields, while the periodic boundary condition is imposed in the x direction. The background plasma density increases linearly in a negative y-direction as shown in Fig. 1. The high density at $y = 0$ is 300 particles in a cell, while the low-density region at $y = 0$ is 100 particles in a cell. There are about 12 million uniformly distributed electron-proton pairs in the system, which are keeping the charge neutrality. The beam protons with the velocity of $-0.27c$ are added near the low-density region ($5000 < y < 6000$). The average numbers of the beam protons in a cell is about 5 particles. The beam proton velocity corresponds to about $30V_A$ where the Alfvén velocity is 0.0093c. The proton temperature is equal to the electron temperature. Other parameters are as follows: the time step $\omega_{pe}\Delta t = 0.05$($\omega_{pe}$ is defined by using the number density 100/cell at $y = 6000$), mass ratio $m_i/m_e = 1836.0$, Debye length $v_{th,e}/\omega_{pe} = 1.0\Delta$ (the electron thermal velocity is taken as $v_{th,e} = 0.1c$), and the collisionless skin depth $c/\omega_{pe} = 10\Delta$. The physical quantities associated with the magnetic field B_0, like plasma beta, electron Larmor radius, and ion Larmor radius, are 1/8, 2.5Δ, and 107.1Δ, respectively. We did two simulations with different magnetic field strengths. The first simulation is that the ratio of ω_{ce} to ω_{pe} at $y = 6000$ is 0.4. The second is that to simulate the deep photospheric region where the magnetic field is strong, we take the strength of the magnetic field to be four times greater than in the first case. Therefore the ratio of ω_{ce} to ω_{pe} at $y = 6000$ is 1.6, and the plasma beta, electron Larmor radius, and ion Larmor radii are 1/128, 0.625Δ, and 26.8Δ, respectively.

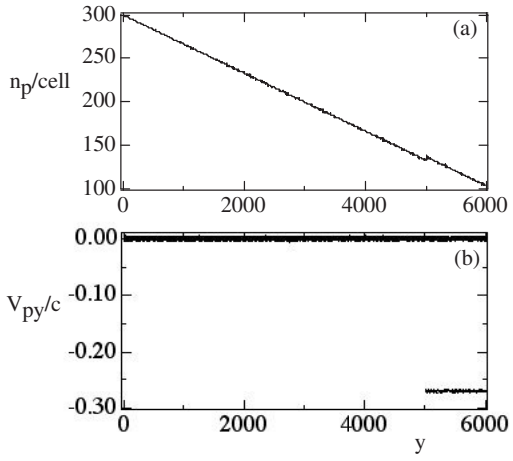

Fig. 1. (a) The initial proton density distribution and (b) the initial proton phase-space ($V_{py}-y$) plot. The proton beam with a negative velocity of $0.27c$ in the y-direction is located at $5000 < y < 6000$ in the low-density region.

Finally we investigate how the emission process of the electromagnetic waves depends on the angle between the magnetic field and proton beams for the same parameters as the first simulation case of $\omega_{ce}/\omega_{pe} = 0.4$.

3. Simulation results

First of all, we show how the proton beams propagate along a uniform magnetic field for the case of $\omega_{ce}/\omega_{pe} = 0.4$. In Fig. 2a we show the plot of the initial electron phase-space ($V_{ey}-y$) and in Fig. 2b the initial proton phase-space ($V_{py}-y$) plot. In Figs. 2c and d the electron and proton phase-space plots at $\omega_{pe}t = 1500$ are shown. As seen in Fig. 2d the proton beams propagate in the negative y-direction almost without losing their kinetic energy,

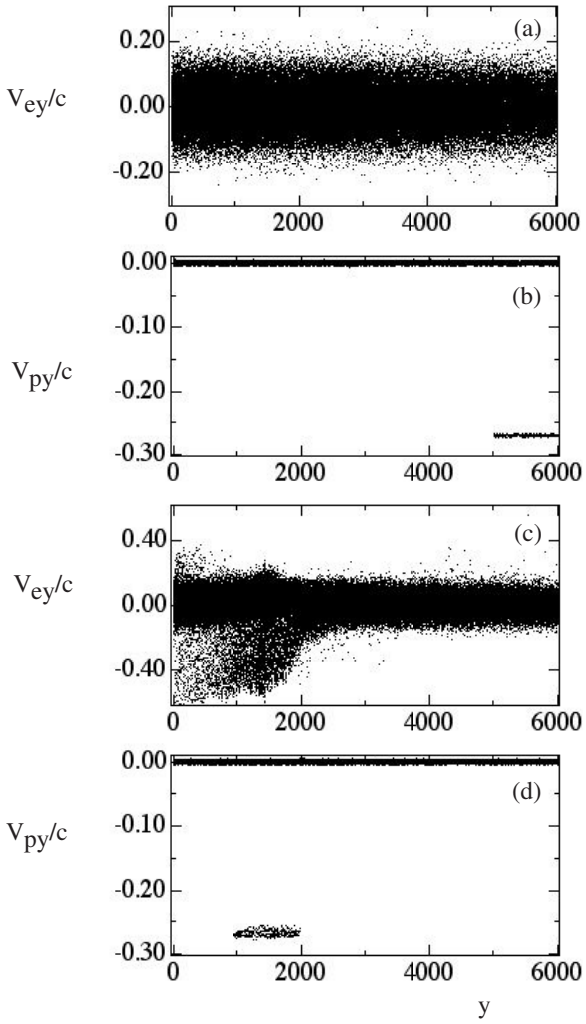

Fig. 2. a) The initial electron phase space ($V_{ey} - y$) plot and **b)** the initial proton phase space ($V_{py} - y$) plot. The electron **c)** and proton phase space **d)** plots at $\omega_{pe}t = 1500$.

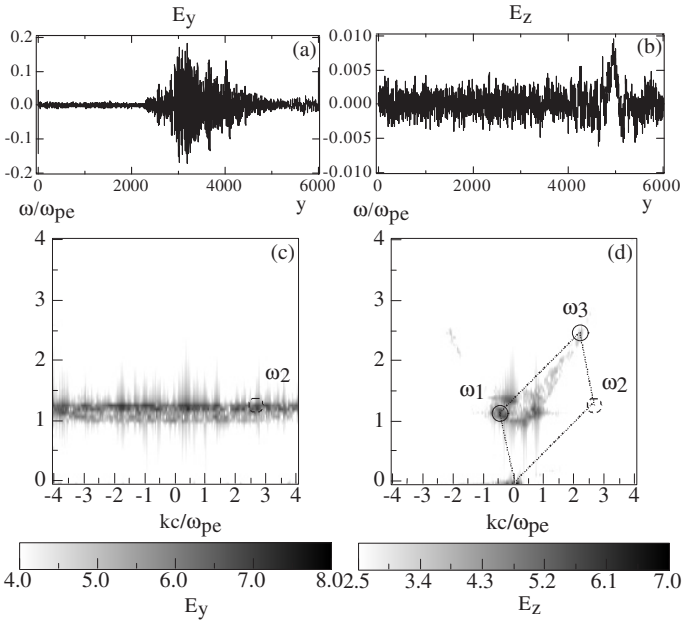

Fig. 3. a) The spacial structures of electrostatic electric field E_y and **b)** E_z at $\omega_{pe}t = 800$. **c)** The dispersion relation of the electrostatic field E_y that was obtained from space-time Fourier transformation taken in the region of $3952 < y < 6000$ and $800 < \omega_{pe}t < 902.4$. The proton-beam mode and Langmuir waves are excited. **d)** The dispersion relation of the electromagnetic waves E_z that was obtained from space-time Fourier transformation taken in the region of $3952 < y < 6000$ and $800 < \omega_{pe}t < 902.4$.

while some background electrons tend to move, together with proton beams, to keep the charge neutrality, and some fraction of the electrons are accelerated in the front of the proton beams. The electron acceleration at the front end of the proton beam is due to electron trapping by the electrostatic waves that are driven by the proton beam. The work by Dieckmann et al. (2006) discusses this in detail, and it shows a high-resolution animation of this electron pick-up.

To understand what is happening during the interaction between proton beams and background electrons, we analyze the electric fields by using two-dimensional, space and time Fourier transformation during the early phase of the interaction. All data for the electric fields are taken at $x = 5\Delta$. The spatial structures of the electrostatic electric fields E_y and E_z at $\omega_{pe}t = 800$ are shown in Figs. 3a and b, respectively. Figure 3c shows the dispersion relation of the electrostatic field E_y that was obtained from space-time Fourier transformation taken in the region of $3952 < y < 6000$ and $800 < \omega_{pe}t < 902.4$. It is seen that the Langmuir waves are excited. Figure 3d shows the dispersion relation of the electromagnetic waves E_z, which was obtained from space-time Fourier transformation taken in the region of $3952 < y < 6000$ and $800 < \omega_{pe}t < 902.4$. We find that, in the same direction as the proton beams, two modes are strongly excited. The upper and lower mode show the R-mode and L-mode, respectively. The cut-off frequencies of the R- and L-modes are given by the following expressions, respectively;

$$\omega_R = 0.5\omega_{ce}\left[\left(1 + 4\omega_{pe}{}^2/\omega_{ce}{}^2\right)^{1/2} + 1.0\right], \quad (1)$$

$$\omega_L = 0.5\omega_{ce}\left[\left(1 + 4\omega_{pe}{}^2/\omega_{ce}{}^2\right)^{1/2} - 1.0\right]. \quad (2)$$

We also find from Fig. 3d that back-scattered electromagnetic waves occur and propagate to positive y-direction. The strong emission occurs close to the same frequency as the Langmuir waves, while the second harmonic wave shown by ω_3 in Fig. 3d is also excited. The excitation mechanism of the fundamental electromagnetic waves is that proton beams drive the electron flow to keep the charge neutrality, resulting in the excitation of Langmuir waves as seen in Fig. 3c. Due to the density inhomogeneity, the electromagnetic waves with R and L modes can be generated with almost the same frequency with local Langmuir wave frequency by the linear mode conversion. The second harmonic wave ω_3 in Fig. 3d is excited by the nonlinear three-wave coupling, $\omega_3 = \omega_1 + \omega_2$, where ω_1 is the forward L-mode shown in Fig. 3c and ω_2 should be the back-scattered Langmuir wave shown in Fig. 3c. The simulation by Dieckmann et al. (2006) has not revealed any electromagnetic wave generation. This is further evidence to support our statement that the wave-energy conversion is due to the plasma density gradient in our simulation.

In Fig. 4a we show the velocity distribution functions of the electron and proton at $\omega_{pe}t$ =0, while in Fig. 4b we show the velocity distribution functions of the electron and proton at $\omega_{pe}t = 1500$. During the interaction between proton beams and background plasma, proton beams can propagate almost

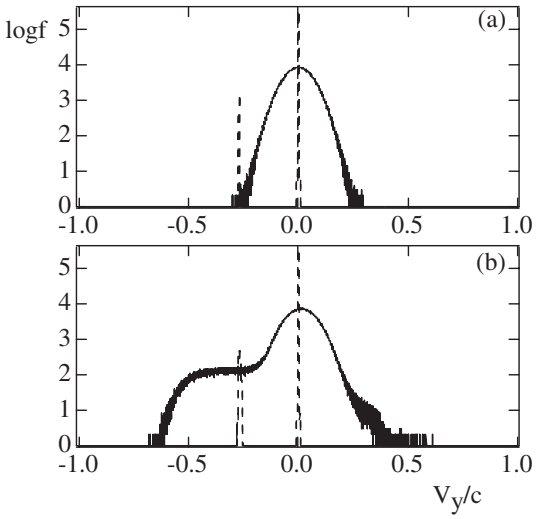

Fig. 4. a) The velocity distribution functions of the electron (solid line) and proton (dashed line) at $\omega_{pe}t = 0$. **b)** The velocity distribution functions of the electron (solid line) and proton (dashed line) at $\omega_{pe}t = 1500$.

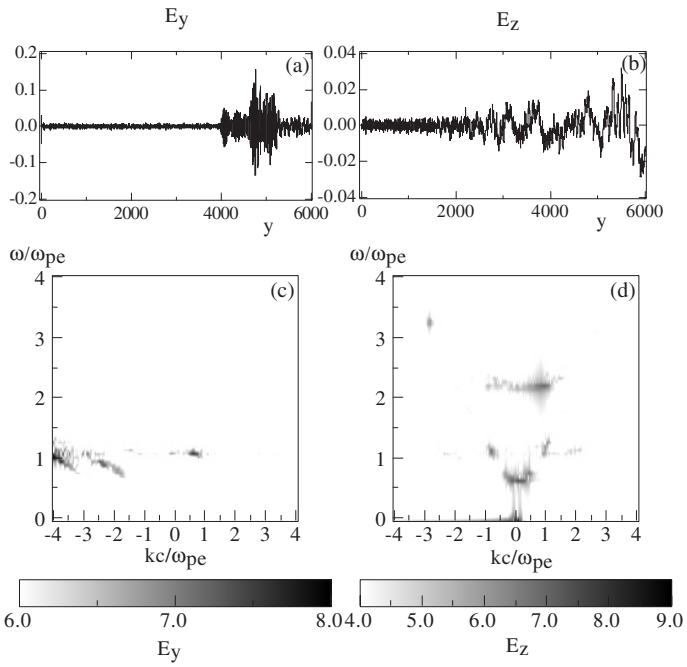

Fig. 5. a) Snapshot of electrostatic field E_y at $\omega_{pe}t = 400$ associated with Langmuir waves. **c)** Dispersion relation of E_y for $\omega_{ce}/\omega_{pe} = 1.6$, which is obtained from the data E_y of $3952 < y < 6000$ and $400 < \omega_{pe}t < 502.4$. **b)** Snapshot of electric field E_z at $\omega_{pe}t = 750$ associated with electromagnetic waves. **d)** Dispersion relation of E_z for $\omega_{ce}/\omega_{pe} = 1.6$, which is obtained from the data E_z of $3952 < y < 6000$ and $750 < \omega_{pe}t < 852.4$.

without damping and can emit the electromagnetic waves. The background electrons are accelerated to keep the charge neutrality, resulting in the excitation of Langmuir waves. The excited Langmuir waves can be transformed to the electromagnetic waves propagating both forwards and backwards. Our simulations prove a plateau distribution of electrons, centred at the proton beam speed. This plateau is due to trapping and is identical to what is found by Dieckmann et al. (2006).

Next we investigate the emission process of electromagnetic waves when the proton beams propagate into the strong magnetic field region ($\omega_{ce}/\omega_{pe} = 1.6$) of the deep photosphere. The spatial structures of the electrostatic electric field E_y at $\omega_{pe}t = 400$ and E_z at $\omega_{pe}t = 750$ are shown in Figs. 5a and b, respectively. Figure 5c shows the dispersion relation of the electrostatic field E_y that was obtained from space-time Fourier transformation taken in the region of $3952 < y < 6000$ and $400 < \omega_{pe}t < 502.4$. It is seen that Langmuir waves and beam modes are excited. The work by Dieckmann et al. (2006) demonstrates that the flow-aligned magnetic field is strong enough to suppress the growth of the filamentation instability. Thus, an Ey electric field component can only originate from the Langmuir waves. Otherwise Ey may have contributions from obliquely propagating waves.

Figure 5d shows the dispersion relation of the electromagnetic wave E_z that was obtained from space-time Fourier transformation taken in the region of $3952 < y < 6000$ and $750 < \omega_{pe}t < 852.4$. We find that two modes are strongly excited in the reverse direction to the proton beams. The intensity of the excited modes is about two orders of magnitude higher than the previous weak magnetic field case ($\omega_{ce}/\omega_{pe} = 0.4$). The upper and lower modes show the R-mode and L-mode, respectively. In Fig. 6 we show the theoretical dispersion relation of R and L modes in cold plasmas, which satisfy the following dispersion relation,

$$\left(\frac{kc}{\omega}\right)^2 = 1 - \frac{{\omega_{pe}}^2}{\omega(\omega_{ce} \pm \omega)} \tag{3}$$

where + and − correspond to the L and R modes, respectively. The excited R and L modes are located between two theoretical curves. The intensity of the R mode is comparable to and slightly

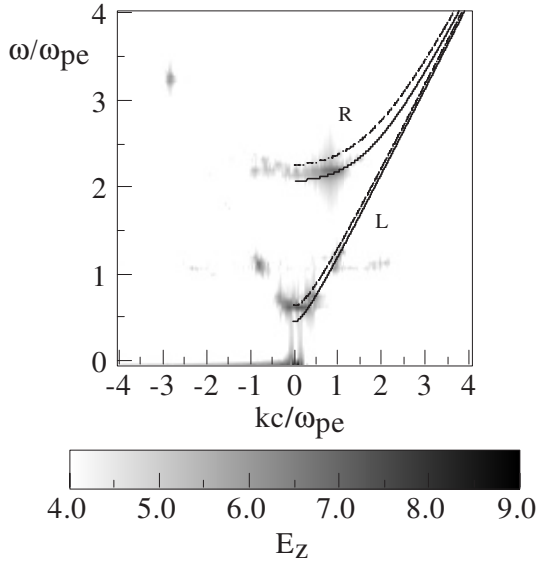

Fig. 6. Dispersion relation of electromagnetic waves for $\omega_{ce}/\omega_{pe} = 1.6$, obtained from the data E_z of $3952 < y < 6000$ and $750 < \omega_{pe}t < 852.4$. Theoretical dispersion relations for R-mode and L-mode are shown by solid lines for $n_0 = 100$ and dashed lines for $n_0 = 150$.

less than that of L mode. The L mode could correspond to the 212 GHz emission and the R mode to the 405 GHz emission. These simulation results could be applied to the electromagnetic wave emission by Kaufmann et al. (2004), which shows the terahertz range from the solar photosphere during the solar flares.

Finally we investigate how the emission process of the electromagnetic waves depends on the angle between the magnetic field and proton beams for the same parameters as the

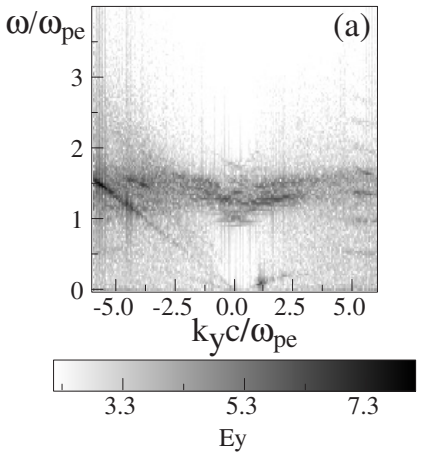

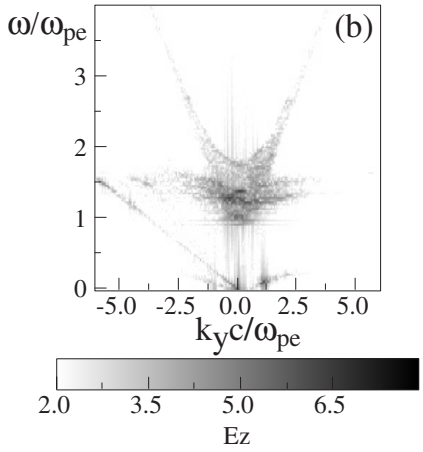

Fig. 7. Dispersion relation of electromagnetic waves for oblique propagation (45°), obtained from the data **a)** E_y and **b)** E_z of $1000 < y < 5096$ and $1200 < \omega_{pe}t < 1404.8$.

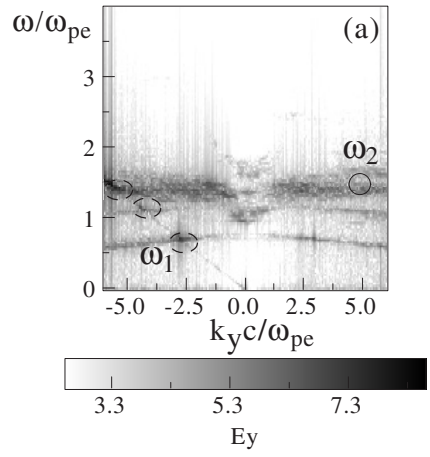

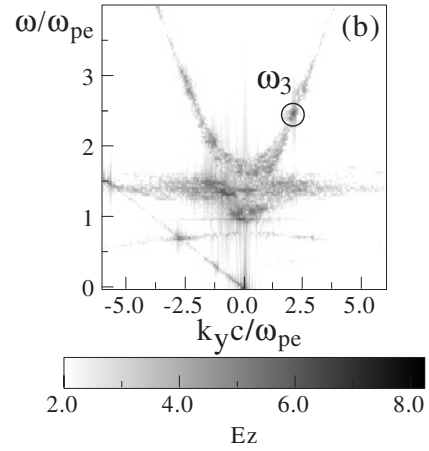

Fig. 8. Dispersion relation of electron Bernstein waves and electromagnetic waves for perpendicular propagation, as obtained from the data **a)** E_y and **b)** E_z of $1000 < y < 5096$ and $1200 < \omega_{pe}t < 1404.8$. The three dashed circles in **a)** show three harmonics of electron Bernstein waves coupled with the proton-beam mode. The extra-ordinary wave (ω_3) can be excited from two Bernstein waves (ω_2 and ω_1) in **a)** through three-wave interactions.

first simulation case. First we show the case of the external magnetic field ($B_x = B_y$) where the proton beams propagate to the y-direction at the angle of 45° from the external magnetic field. Figure 7 shows the dispersion relation of electromagnetic waves for oblique propagation (45°), which is obtained from the data (a) E_y and (b) E_z of $1000 < y < 5096$ and $1200 < \omega_{pe}t < 1404.8$. In Fig. 7a we find the excitation of two modes: the proton-beam mode propagating in the same direction as the proton beams and the obliquely propagating Langmuir wave (Z-mode) whose theoretical dispersion relation is given by $\omega^2=\omega_{pe}{}^2+\omega_{ce}{}^2 \sin^2\theta+3k^2v_{th,e}{}^2$. As seen in Fig. 7b the electromagnetic waves appears with the same frequency as the excited Z-mode propagating behind the proton beams. The excitation mechanism of the electromagnetic waves is due to the linear direct-mode conversion from the Z-mode. The high-frequency electromagnetic waves are also weakly excited.

We show the case of perpendicular propagation where the external magnetic field is in the x-direction and the proton beams propagate in the y-diretion. Figure 8 shows the dispersion relation of electron Bernstein waves and electromagnetic waves for perpendicular propagation, which is obtained from the data (a) E_y and (b) E_z of $1000 < y < 5096$ and $1200 < \omega_{pe}t < 1404.8$. Three dashed circles in Fig. 8a show three harmonics of electron Bernstein waves (Crawford 1965) coupled with the proton beam mode. The extra-ordinary (X) mode (ω_3) in Fig. 8b can be excited from two Bernstein waves (ω_2 and ω_1) in Fig. 8a through three-wave interactions. The high cutoff frequency of the X mode is about $1.36\omega_{pe}$ and the lower cutoff frequency of the X-mode is about $0.92\omega_{pe}$ for $\omega_{ce} = 0.4\omega_{pe}$, while the upper hybrid frequency $\omega_{UH} = (\omega_{pe}{}^2 + \omega_{ce}{}^2)^{1/2}$ is about $\omega_{UH} = 1.18\omega_{pe}$. The same nonlinear excitation of the X-mode by two electron Bernstein waves, as the present case was investigated during pinching current sheet (Haruki & Sakai 2001).

We may conclude that the electromagnetic waves can be excited behind the proton beams, almost independent of the direction of the uniform magnetic field, although the emission process is different in its details.

4. Discussion and conclusions

We investigated the emission process of the electromagnetic waves by proton beams propagating along and across a uniform magnetic field in nonuniform solar plasma, paying attention to the emission process of electromagnetic waves within the terahertz range from the solar photosphere. The aim was to understand a new solar burst component emitting in the terahertz range during the solar flare observed by Kaufmann et al. (2004). From the simulation where the proton beams propagate into the high-density region along a uniform magnetic field, we found that strong electromagnetic waves are generated behind the proton

beams. When the proton beams propagate perpendicular to the magnetic field, we find that the extra-ordinary mode can be excited from two electron Bernstein waves through three-wave interactions. We also found for the proton beams parallel to the strong magnetic field that the higher-frequency emission like 405 GHz, which originates from a strong magnetic field region has comparable intensity to the 212 GHz emission.

We assumed here the presence of a small-scale density gradient to enhance the wave emission. We need to explore the origin of the small-scale density gradient. The photospheric plasma is probably less strongly magnetized ($\omega_{pe} \gg \omega_{ce}$) than what has been discussed here. But the simulation results for the weak magnetic field case ($\omega_{pe} \gg \omega_{ce}$) could be applicable to the photospheric plasma.

Acknowledgements. The authors thank the anonymous referee for useful comments that improved on our original paper.

References

Aschwanden, M. J. 2002, Space Sci. Rev., 101, 1
Brown, J. C., Karlicky, M., Mandzhavidze, N. & Ramaty, R. 2000, ApJ, 541, 1104
Buneman, O. 1993, in Computer Space Plasma Physics, Simulation Techniques and Software, ed. H. Matsumoto & Y. Omura (Tokyo: Terra Scientific), 67
Crawford, F. W. 1965, Radio Science, 69D, 789
Dieckmann, M. E., Shukla, P. K., & Eliasson, B. 2006, New J. Phys., 8, 225
Forrest, D. J. & Chupp, E. L. 1983, Nature, 305, 291
Haruki, T. & Sakai, J. I. 2001, ApJ, 552, L175
Katsouleas, T. & Dawson, J. M. 1983, Phys. Rev. Lett., 51, 392
Dieckmann, M. E., & Shukla, P. K. 2006, PPCF, 48, 1515
Kaufmann, P., & Raulin, J.-P. 2005, Eos. Trans. AGU, 86(18), Jt. Assem. Suppl. Abstract SH54A-06
Kaufmann, P. et al. 2001, in Proc. SBMO/IEEE MTT-S Int. Microwave and Optoelctronics Cof., ed. J. T. Pinho, G. P. Santos Cavalcante, & L. A. H. G. Oliveira (Piscataway: IEEE), 439
Kaufmann, P., Raulin, J.-P., Gimenez De Castro, C. G., Levato, H. et al. 2004, ApJ, 603, L121
Sagdeev, R. Z., & Shapiro, V. D. 1973, JETP Letters, 17, 279
Saito, S., & Sakai, J. I. 2004a, ApJ, 616, L179
Saito, S., & Sakai, J. I. 2004b, Phys. Plasmas, 11, 5547
Saito, S., & Sakai, J. I. 2006, ApJ, 652, 793
Sakai, J. I., & Ohsawa, Y. 1987, Space Sci. Rev., 46, 113
Sakai, J. I. , & de Jager, C. 1996, Space Sci. Rev., 77, 1
Sakai, J. I., & Nagasugi, Y. 2007, ApJ, submitted
Sakai, J. I., Mori, T., & Saito, S. 2005, A&A, 442, 687
Sakai, J. I., Mori, T., Saito, S., Tanaka, Y., & Aurass, H. 2006a, A&A, 454, 983
Sakai, J. I., Nagasugi, Y. Saito, S., & Kaufmann, P. 2006b, A&A, 457, 313
Tajima, T., Brunel, F., & Sakai, J. I. 1982, ApJ, 245, L45
Ucer, D., & Shapiro, V. D. 2005, Phys. Lett. A, 346, 163